Ore-forming fluids in the Grübler orebody, Idrija mercury deposit, Slovenia

Autor(en): **Palinkaš, Ladislav / Strmi, Sabina / Spangenberg, Jorge**

Objekttyp: **Article**

Zeitschrift: **Schweizerische mineralogische und petrographische Mitteilungen = Bulletin suisse de minéralogie et pétrographie**

Band (Jahr): **84 (2004)**

Heft 1-2: **Geodynamics and Ore Deposit Evolution of the Alpine-Carpathian-Balkan-Dinaride Orogenic System**

PDF erstellt am: **30.06.2024**

Persistenter Link: https://doi.org/10.5169/seals-63745

Schweizerische Mineralogische und Petrographische Mitteilungen 84, 173–188, 2004

Ore-forming fluids in the Grübler orebody, Idrija mercury deposit, Slovenia

Ladislav Palinkaš[1], *Sabina Strmić*[1], *Jorge Spangenberg*[2], *Walter Prochaska*[3] and *Uroš Herlec*[4]

Abstract

Fluid inclusions in cinnabar, quartz and barite from the Grübler orebody of the giant Idrija mercury deposit in the NW Dinarides of Slovenia were studied by microthermometry, laser Raman spectrometry, and bulk crush-leach analysis using ion chromatography and atomic absorption spectrometry. They homogenise at T_h = +160 to +180 °C and their salinity ranges from 2.6–12.8 wt% NaCl eq. Low eutectic temperatures (T_e, average –52 °C) indicate the presence of divalent cations (Mg, Ca), as confirmed by crush-leach analysis. Fluid-chemical geothermometers revealed temperatures of 206–265 °C (Na/K), 183 °C (Na/Li), and 172–220 °C (Na/K/Ca). Laser Raman spectrometry found no other volatiles than water and confirmed dolomite as solid inclusions and daughter minerals within fluid inclusions. Solid inclusions of cinnabar in quartz and barite point to co-precipitation of these three minerals. The $\delta^{34}S$ is between –0.7 and +1.5‰ (V-CDT) for cinnabar. Barite has $\delta^{34}S$ between +45.6 and +56.3‰ and probably precipitated later out of isotopic equilibrium with the sulphides. Geology, fluid inclusion and isotope data indicate that the deeper parts of the Idrija deposit formed by hydraulic fracturing in a Middle Triassic rift basin, in a hydrothermal system driven by subjacent basaltic intrusions. Fluid overpressure, leading to local fluidisation of breccia fragments, may have been aided by hydrothermal maturation of the organic matter in the rift sediments, as indicated by abundant bituminous matter in the vein- and breccia-hosted cinnabar ore. Sulphur in cinnabar was derived from a possible magmatic component and a sulphide contribution derived by reduction of local sulphate. The latter contribution increased upward towards the sediment surface, where high-grade syn-diagenetic cinnabar and possibly some primary metallic Hg were deposited beneath a marsh environment.

Keywords: Idrija mercury deposit, fluid inclusions, S-isotopes, Dinarides, Triassic rifting.

1. Introduction

There are two world-class mercury ore deposits regarding total reserves and production: Almadén (Spain) and Idrija (Slovenia). Of the total world production to date (800.000 tons of mercury), Almadén has produced 35% (280.000 tons; Hernández, 1999) and Idrija 13% (128.000 tons; Mlakar, 1974). Idrija still contains 10% of the world's known mercury reserves (Brinck and van Wambeke, 1975). It is characterised by epigenetic, hydrothermal cinnabar veins, stockworks, impregnations and massive replacements in Upper Paleozoic and Lower Triassic sediments, which are probably coeval with syngenetic, sedimentary-exhalative cinnabar ore formed in overlying Middle Triassic strata (Drovenik et al., 1980). The driving force for hydrothermal fluid flow was the elevated geothermal gradient related to Middle Triassic rifting with widespread bimodal volcanism (Pamić, 1984). The Almadén deposit is also related to rifting and submarine basaltic magmatism, in the early Palaeozoic, but its genesis is more complex due to later regional metamorphism. Three lenticular strata-bound cinnabar impregnations in the Early Silurian Criadero quartzite occur adjacent to epigenetic hydrothermal mineralisation in the Frailesca phreato-magmatic explosion breccia, a diatreme piercing the quartzites (Soupé, 1990; Hernández et al., 1999). Both mercury deposits contain abundant organic-rich shales. Fluid inclusion studies on quartz and dolomite co-precipitated with cinnabar at Almadén gave salinities of 1–13 wt% NaCl eq., and T_h = 85–240 °C (Iglesias and Pérez, 1989; Higueras et al., 1999). The geology and genesis of the Idrija deposit attracted

[1] University of Zagreb, Faculty of Sciences, Geology department, 10000 Zagreb, Croatia. <lpalinka@public.srce.hr>
[2] Université de Lausanne, Institut de Minéralogie et Géochemie, BFSH2, Lausanne, Switzerland. <Jorge. Spangenberg@img.unil.ch>
[3] University of Leoben, Mineralogy and Petrology, Institute of Geosciences, Leoben, Austria. <prochask@unileoben.ac.at>
[4] University of Ljubljana, Department of Geology, Ljubljana, Slovenia. <uros_herlec@ntfgeo.uni-lj.si>

0036-7699/04/0084/173

the attention of many researchers over the past two centuries. Schrauf (1891), Berce (1958) and Mlakar (1967, 1969) advocated an epigenetic origin in Triassic time, while Stur (1872), Kossmat (1911), Tornquist (1930) and Colbertaldo and Slavik (1961) favoured ore formation in the Tertiary.

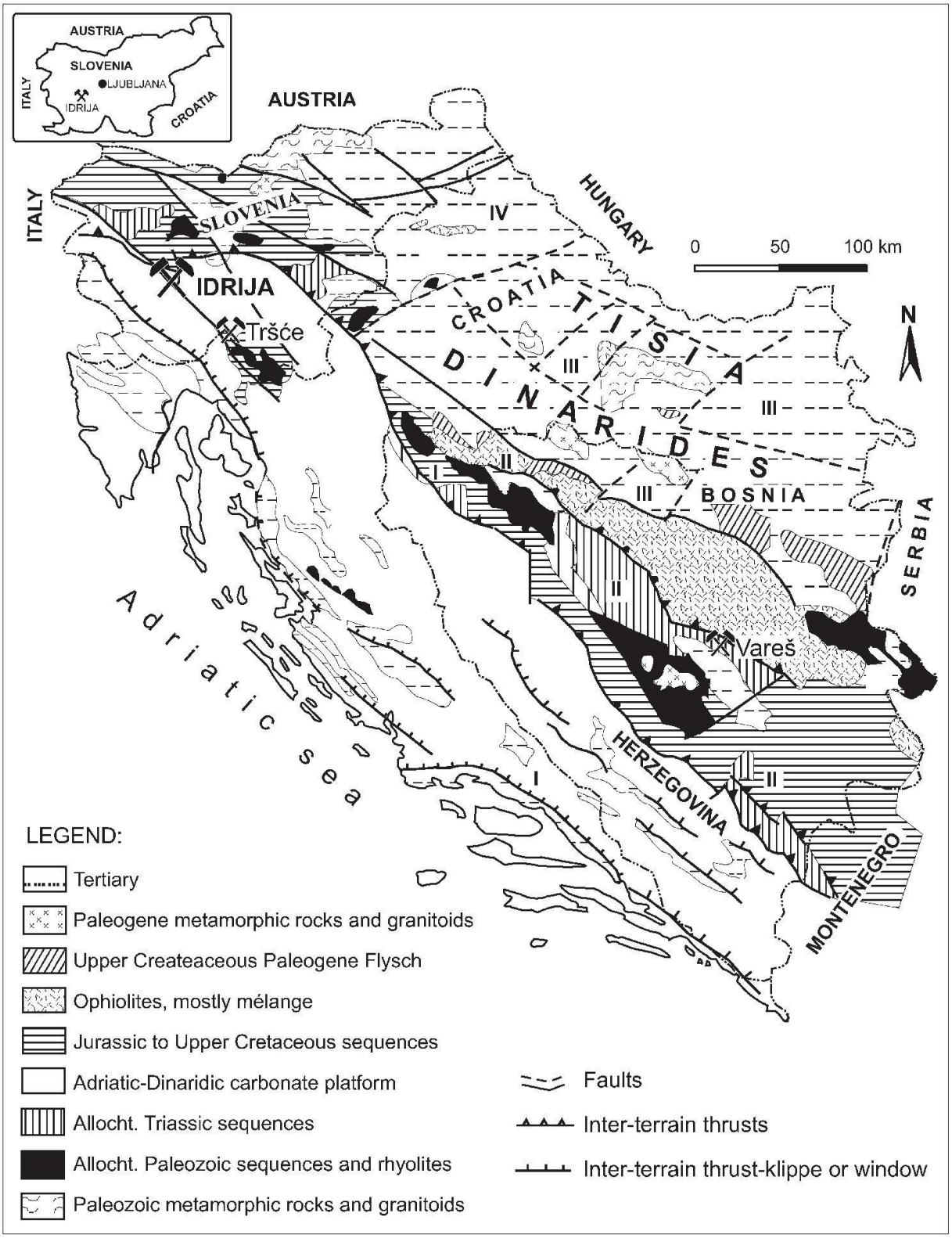

Fig. 1 Geological sketch map of the Central and Northwest Dinarides; I—External Dinarides; II—Internal Dinarides; III—Pannonian Basin underlain by Tisian basement; IV—Zagorje-Mid-transdanubian zone (from Pamić and Jurković, 1997). The Dinarides consists of four geotectonic units aligned NW–SW from a carbonate platform in the Southwest to subduction-related formations confronting the Tisia ensialic block in the Northeast (see text). Middle Triassic advanced Tethyan rifting is recorded in a Triassic volcano-sedimentary unit aligned parallell to the other principal units, with numerous SEDEX deposits including three major Hg-only deposits: Idrija, Tršće and Draževići in the Vareš district. Others occur in the same Triassic formation outside of the map area in the SE Dinarides.

Mlakar and Drovenik (1971) were the first to distinguish epigenetic-hydrothermal and stratiform ore types within the Permotriassic sedimentary sequence.

Numerous papers have been published on the geology and genesis of both deposits (e.g., Placer, 1976; Drovenik et al., 1980; Čadež et al., 1981; Čar, 1990; Drovenik et al., 1991; Mlakar, 1996; Saupé, 1990; Saupé and Arnold, 1992; Hernández et al., 1999; Lavrić and Spangenberg, 2003), but there is a lack of data on the ore-forming fluids particularly for Idrija. In this paper, we present fluid inclusion and S-isotope data for cinnabar, barite and quartz from the epigenetic Grübler orebody, situated in the basal part of the Idrija deposit where ascending fluids started to precipitate cinnabar.

2. Geology and mineralisation

2.1. Regional geology and tectonics

The Dinarides (Fig. 1) are an orogenic belt extending along the northeastern margin of the Adriatic microplate (Dewey et al., 1973) or Apulia (Dercourt et al., 1986). The Alpine Wilson cycle, related to opening and closure of the Tethys ocean, developed a regular pattern of geotectonic units aligned from NW to SE. From the Adriatic microplate towards stable Europe in the NE, four units with distinct Mesozoic and Tertiary lithostratigrapy can be distinguished (Fig. 1): (i) the Adriatic-Dinaridic carbonate platform of the Adriatic -Apulian passive continental margin (External Dinarides); (ii) carbonate-clastic formations (flysch); (iii) ophiolites related to Tethyan oceanic crust; (iv) and a sedimentary-magmatic-metamorphic complex of the active European continental margin (Internal Dinarides; Pamić, 1993). In the NW Dinarides, these geotectonic units are condensed. Orogenic compression in the Dinarides resulted from indentation of the Adriatic plate into the European plate (Neubauer et al., 2000), causing extensive overthrusting of complex nappe systems with total slips of tens of km and multiple stacking. The most important one is the Sava nappe consisting of Palaeozoic to Triassic rocks, which extends northwestward into the Southern Alps, and southward across the Central and Southeastern Dinarides into the Hellenides.Triassic rifting near the onset of opening of the Tethys generated a major province of Hg-enriched ore deposits including the giant mecury deposit of Idrija, smaller Hg-only deposits such as Tršće and Draževići, but also essentially coeval sedimentary-exhalative to diagenetic deposits of siderite, base metals and barite commonly containing minor Hg-enrichment. For example, the Middle Triassic tuffs, cherts, shales, sandstones and carbonate sediments of the Vareš region (Central Bosnia) contain deposits of siderite, hematite, manganese oxides, galena, Hg-rich-sphalerite, pyrite, chalcopyrite, barite, and cinnabar (Jurković and Pamić, 1999; Jurković and Palinkaš, 2002). The monomineralic mercury deposit of Draževići, (Ramović et al., 1979) is associated with polymetallic deposits such as Borovica, Vareš, Veovača, and Čevljanovići, which are also rich in mercury.

Idrija and all of these minor deposits are located at the edge of the Adriatic-Dinaridic carbonate platform, developed within volcano-sedimentary series with intermittent carbonate deposition from the Late Permian to the Late Triassic (Mioč, 2001). The Lower and Middle Triassic formations in the Idrija region are products of shallow water sedimentation. The Lower Scythian coarse-grained dolostones, shales and oolitic limestones, Upper Scythian coarse-grained dolostones and sandy shales, and Anisian dolostones are unconformably situated above Permo-Carboniferous organic-rich black shales, Upper Permian sandstones (named Gröden), shales and dolostones with evaporites including gypsum (Fig. 2, simplified after Placer and Čar, 1977). During the Middle Triassic time (Langobardian substage, Ladinian), incipient rifting gave rise to a trough developing along normal faults. Intensive tectonic activity accompanied by volcanism led to deposition of conglomerates, olistostromes, and pyroclastic rocks, followed by syngenetic ore deposition. Within the deposit itself only pyroclastic and epiclastic sediments are present. With continued sedimentation, the fault trough became shallower and was eventually covered by bog sedimentation spread over a wide region. A brackish marshy environment is indicated by fossil flora remnants. Intermittent volcanic activity produced tuffs, tuffites, and cherts interbedded with variably altered basaltic flows (Placer and Čar, 1977).

2.2. Idrija deposit geology

Mercury mineralisation occurs in all rocks from the Permo-Carboniferous to the Upper Ladinian as two main ore types (Drovenik et al., 1980):

(1) Epigenetic veins, stockworks, stringers, impregnations and open-space fillings within clastic sedimentary rocks, and metasomatic replacements and breccia cement within fractured dolomites and limestones. The host rocks comprise all lithotypes from the Permo-Carboniferous to the Upper Ladinian. The orebodies are close to nor-

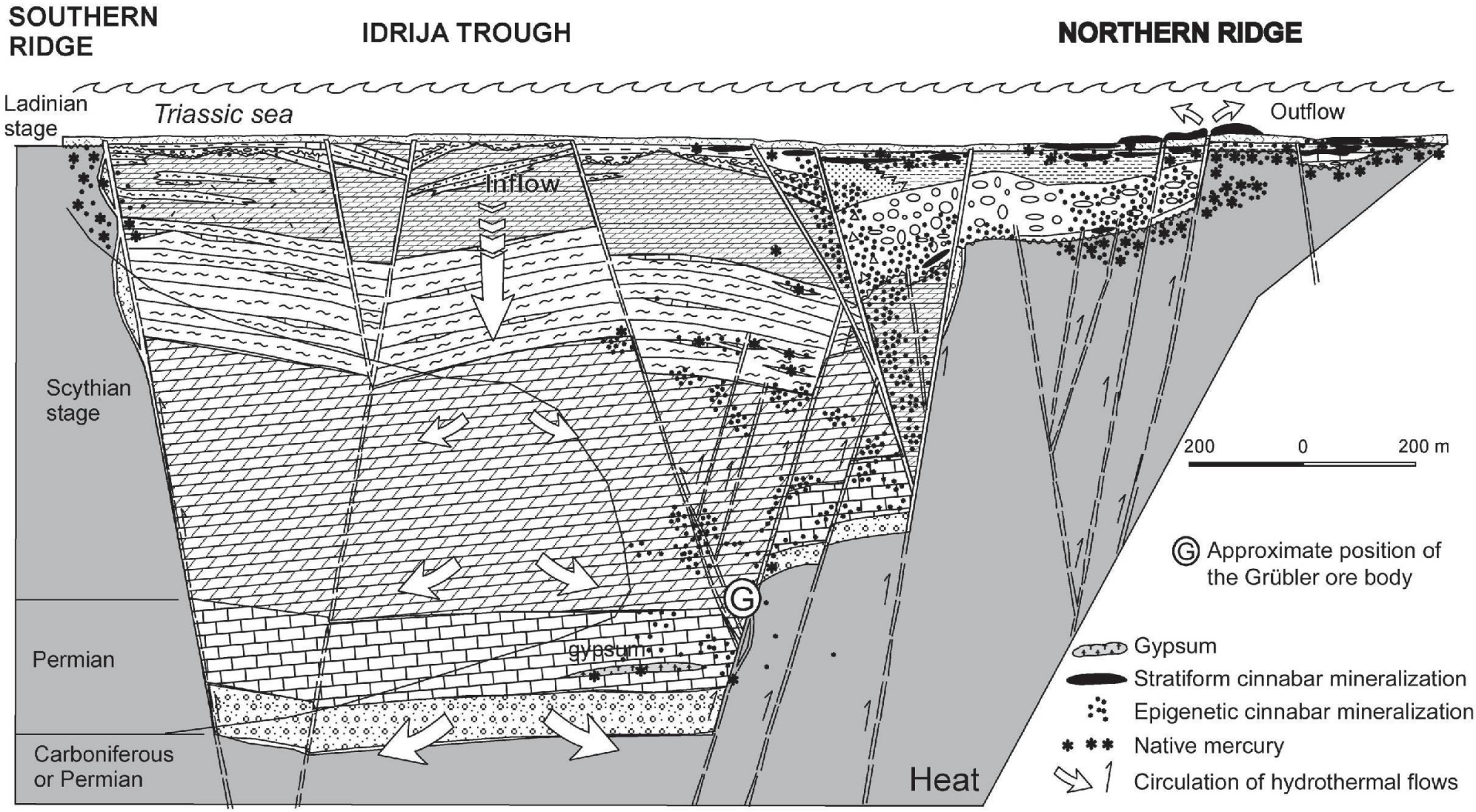

Fig. 2 Schematic reconstruction of the Middle Triassic through during deposition of the Langobardian sediments (modified after Placer and Čar, 1977) showing a conceptual model for the mercury-mineralising palaeogeothermal system driven by Triassic rifting and volcanism. Thermal springs, issuing mercury-bearing fluids into a brackish euxinic basin in a marsh environment deposited rich stratiform cinnabar ores at the top of the sequence, while epigenetic ores including the Grübler orebody (approximate position G) were formed in the subsurface. Black and white arrows indicate ascending and descending fluids.

mal longitudinal and transverse Middle Triassic faults which acted as conduits for ore-forming fluids. The most favourable sites were permeable or tectonically disintegrated host rocks covered by less permeable shales or pyroclastics, which locally acted as a screen for ascending hydrothermal water.

(2) Rich syngenetic ore bodies embedded in the Langobardian volcano-sedimentary sequence. Distinct textural types of the stratiform ore, like small-scale rhythmic bedding, lamination, early diagenetic thrust faulting, folding, graded bedding of pyrite, cinnabar and bituminous-rich shales, have been descriptively referred to as "steel ore", "brick ore" and "liver ore" (Mlakar and Drovenik, 1971).

The principlal ore mineral in both ore types is cinnabar, accompanied by dolomite, calcite and quartz. Metacinnabar appears occasionally in limestone lenses within Lower Scythian micaceous and calcareous shales together with paragenetically later barite (Placer and Čar, 1977). Native Hg is widespread in Permo-Carboniferous black shales, siltstones and sandstones but exceptionally rare in all other lithotypes. Native-Hg bearing black shales occur marginally in the uppermost parts of the trough (Fig. 2). Sphalerite and orpiment are rare. Pyrite and marcasite have been interpreted mainly to be diagenetic minerals, although some hydrothermal pyrite fills the fault planes (Drovenik et al., 1980). Organic matter occurs in the host rocks and ore as disseminated kerogen, as black solid hydrothermal bitumen, and as greenish idrialite, a complex mixture of polycyclic aromatic hydrocarbons containing nitrogen and sulphur-bearing compounds (Blumer, 1975; Wise et al., 1986; Lavrić and Spangenberg, 2001, 2003). Idrialite is found in the epigenetic ore as void fillings or replacements, as well as in the stratiform ore type (Spangenberg et al., 1999).

2.3. The Grübler orebody

Fluid inclusion studies and S-isotope analyses were performed on samples from the Grübler orebody, one of the richest in the Idrija deposit located near the base of Lower Scythian dolostones. Cinnabar mineralisation is controlled by the Grübler normal fault, striking ENE–WSW and dipping steeply towards NNW, and by subvertical open fissures in the hanging-wall of the Grübler fault (Fig. 3). Placer (1974–75, 1976) and Drovenik et al. (1991) distinguished four types of mineralisation in the Grübler orebody:

(i) pyrite fillings (3–5 cm thick) along the fault plane juxtaposing Permo-Carboniferous and Gröden sandstones with Lower Scythian dark dolomite. Cinnabar occurs sporadically within tiny fissures in the fracture zone.

(ii) open ore fissures (veins) adjacent to the Grübler fault, within the 25–30 m wide fracture zones. Individuell veins are not longer than 30 m and not wider than 4 cm, with mutual spacing of 0.5–3 m. The fissures show symmetric internal zoning and are filled completely or partly with white dolomite crystals, cinnabar, pyrite and black bituminous matter. The ore grade in the veins decreases gradually with distance from the fault.

(iii) rich ore in fissures with replacement of white dolomite and pyrite crystals by cinnabar.

(iv) breccias at the intersection of the vertical veins with the Grübler Fault. Dolomitic rock fragments are cemented by white dolomite, cinnabar, quartz, calcite, dark organic matter, minor pyrite and barite in multiple overgrowth crusts (Drovenik et al., 1991). The minerals occur as euhedral, anhedral and colloform grains up to 5 mm size. The open space between clasts is cemented with the same minerals and shows the same association of organic matter and cinnabar. Locally these breccias contain cavities up to 0.5 m in size containing abraded grains of dolomite, quartz, cinnabar and barite as well as rounded dolomite pebbles up to 5 cm in diameter. This abrasion affected earlier hydrothermal dolomite – cinnabar – quartz – barite crusts, and was overgrown by later crusts of the same euhedral, non-abraded hydrothermal minerals, and well-developed barite crystals as the latest mineral in the paragenetic sequence.

Organic matter is intimately associated and co-precipitated with cinnabar throughout the Grübler orebody (Drovenik et al., 1991). Fine cinnabar crystals, uniformly dispersed, form tiny isolated grains, or fill microcracks in organic matter. Single globules, or rounded patches of organic matter impregnated by fine cinnabar grains, may be enclosed within larger cinnabar grains. Botryoidal organic matter with cinnabar-filled cracks may be surrounded by a younger generation of cinnabar on the scale of a few 100 μm. Drovenik et al. (1991) interpreted the colloform texture of the ore as reflecting co-precipitation of organic matter and cinnabar from a colloidal solution. Alternatively, they may be precipitated from a mixture of hydrothermal fluid and oil or bitumen.

3. Analytical Methods

Fluid inclusion analysis was performed on transparent quartz crystals, irregular cinnabar grains, and white, 0.1–0.2 mm thick barite crystals, collected in a subvertical veins and cavities of the

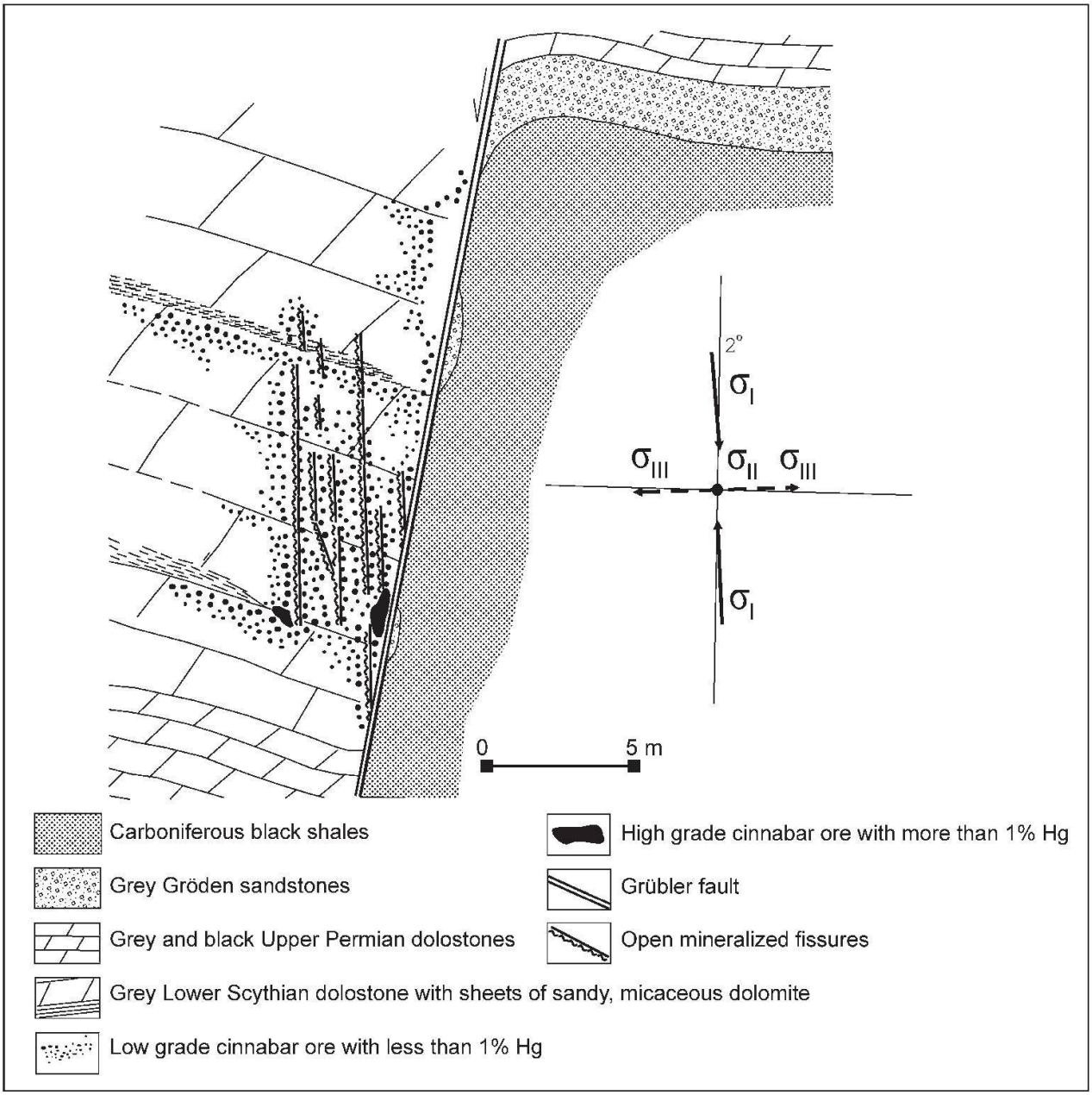

Fig. 3 Section through the Grübler orebody during the Middle Triassic (slightly modified after Placer, 1974–1975). Mineralised fissures opened perpendicular to the lowest main stress σ3 of rift extension. Hydraulic fracturing lead to expulsion of the hot fluid along the main fault and through the fissures into the cold overlying carbonate rocks.

Grübler ore body. The study included abraded mineral grains as well as post-brecciation crystals. Microthermometry, laser Raman spectrometry, and bulk crush-leach analysis of fluid inclusions by ion chromatography and atomic absorption spectrometry was complemented by sulphur isotope analyses on cinnabar and barite.

Microthermometry was performed on doubly-polished wafers (250 μm) using a microscope equipped with *Leitz-Wetzlar P25/0.50* and *UM32/0.30* objectives and a *Chaixmeca* freezing-heating stage. Two synthetic fluid inclusion standards (pure H_2O, mixed H_2O–CO_2) were used for system calibration. The precision was ±2 °C for homogenisation temperature, and ±0.2 °C in the temperature range between –60 and +10 °C.

Laser Raman spectrometry was carried out with a *Dilor LabRAM* with a frequency-doubled *Nd-YAG* green laser (532 nm, 100 mV) focused through an *Olympus* BX microscope. Objective lenses of 50× and 100× magnification, combined with a confocal optical arrangement, enabled a resolution of about one micrometer in horizontal and lateral directions.

Bulk solute compositions of the trapped fluids were analysed by ion chromatography using a technique modified after Bottrell et al. (1988). Cleaned mineral grains (1g of quartz or 2g of barite and cinnabar) were ground with 5 ml of doubly-distilled water in an agate mortar and pestle. The resulting slurry was filtrated to separate the leachate from the sample residue. A *Dionex DX-*

500 system with a micro-membrane suppressor and pulsed amperometric detector was used for analysis of halogens. Cations were analysed from aliquots of the same solutions using standard atomic absorption spectrometry.

Sulphur isotope analyses were performed using an on-line elemental analyser (EA)-continuous flow-isotope ratio mass spectrometer (IRMS). The EA-IRMS system consists of a *Carlo Erba 1108* elemental analyser coupled with a continuous helium flow interface to the *Thermoquest/ Finnigan MAT Delta S IRMS*. Sample compounds were decomposed under helium and oxygen flux by flash combustion in a single oxidation–reduction quartz tube filled with oxidising (tungsten trioxide) and reducing (elemental copper) agents at 1030 °C. Water was removed using anhydrous magnesium perchlorate. The released gases enter a chromatographic column (*Poropak QS*) for separation of SO_2, which is then isotopically analysed (Gieseman et al., 1994). The S-isotope values are reported relative to the *Vienna Canyon Diablo troilite* standard (*V-CDT*). The reproducibility, assessed by replicate analyses of internal laboratory standards (natural pyrite, $\delta^{34}S$ = +6.1‰; synthetic mercury sulphide, $\delta^{34}S$ = +15.5‰; barium sulphate, $\delta^{34}S$ = +12.5‰) was better than 0.2‰.

4. Results

4.1. Petrography of inclusions

Microscopic examination of barite, quartz and cinnabar revealed the following types of fluid inclusions:

(1) Multiphase (L+V+$S_{anis.}$), irregularly shaped, aqueous fluid inclusions (Fig. 4a).

(2) Two-phase (L+V), aqueous inclusions, with progressive growth of negative crystal forms (Fig. 4b).

(3) Two-phase (L+V), aqueous, secondary or pseudosecondary inclusions, aligned along healed fractures.

(4) Monophase, liquid inclusions (L).

(5) Solid inclusions (S).

Inclusions in quartz occur mostly parallel to growth zones (Fig. 4c). These incorporate solid inclusions of carbonates and cinnabar (Figs. 4d and 4e). In most cases, optical identification of the melting phases was not possible within cinnabar specimens due to the small size of the inclusions. Some inclusions of type (2) were measurable (Fig. 4f). The most widespread inclusion in barite is solid cinnabar (Fig. 4g). The degree of fill of all aqueous inclusions varies between 0.80 and 0.95.

4.2. Microthermometry

Inclusions of type (1) and (2) yield fairly uniform results in all investigated minerals, and their cogenetic nature is confirmed by the presence of cinnabar inclusions together with primary fluid inclusions in quartz and barite. Freezing occured between –44 and –57 °C. Eutectic temperatures (T_e) around –52 °C indicate the presence of divalent cations (Fig. 5a). Melting runs in the temperature range between –35 and 0 °C indicate the existence of two hydrates. Melting of the first hydrate ($T_m$hyd1) was recorded in the temperature interval between –34.5 and –27.0 °C (Fig. 5b), whilst the temperature interval for final melting of the second hydrate, $T_m$hyd2, is fairly wide (–25.7 to –20.5 °C, Fig. 5c). The ice melting temperature, $T_m$ice, is between –1.5 and –8.9 °C (Fig. 5d). The fluid salinity was determined from $T_m$ice

Table 1 Calculated fluid inclusions salinities and bulk ion crush-leach analysis of quartz, barite and cinnabar.

	Salinity	**Molality** (mmol/kg)										
	(wt% NaCl equ.)	Li	Na	K	Mg	Ca	Cl	SO_4	Q^+/Q^-	Cl/SO_4	Na/K	Na/Li
quartz	2.6–12.8	0.0	63.1	6.7	427.3	277.7	98.4	22.8	9.7	4.3	9.3	–
barite	4.2–8.9	0.3	131.5	7.9	1022.9	298.2	237.0	74.2	7.0	3.2	16.7	515.5
cinnabar	3.6–9.0	0.0	73.1	6.1	119.1	85.8	158.2	4.4	3.0	34.7	12.0	–

Table 2 Geothermometers Na/K, Na/Li, Na/K/Ca and temperature of homogenisation, T_h.

	T(°C) Na/K*	**T(°C) Na/Ca****	**T(°C) /K/Ca*****	**T_h(°C)**	**Salinity** (wt% NaCl equ.)
quartz	265	–	180	160–218	2.6–12.8
barite	206	183±29	172	–	4.2–8.9
cinnabar	237	–	220	–	3.6–9.0

*After Can (2002); ** after Verma and Santoyo (1997); *** after Fournier and Truesdell (1973)

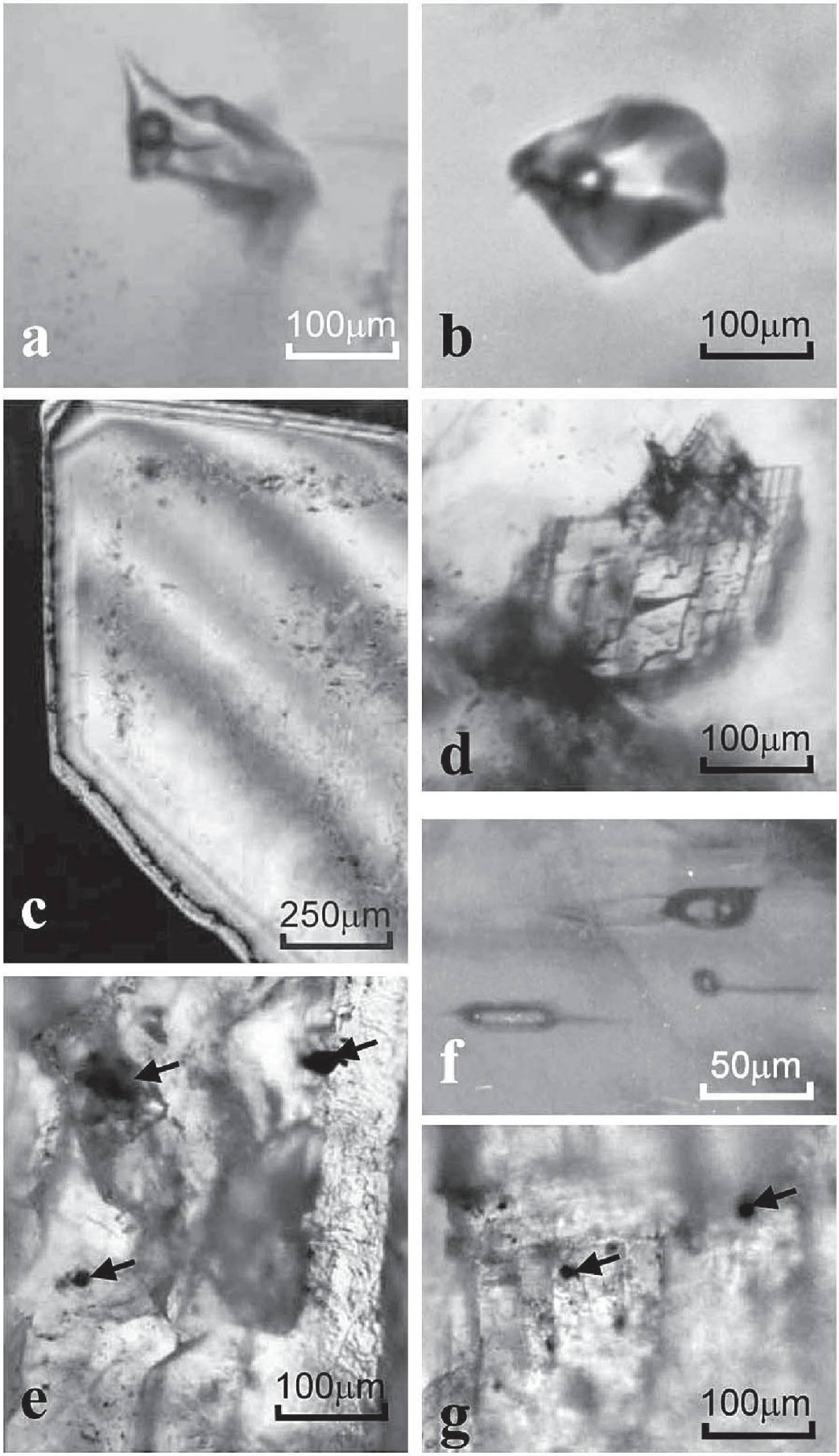

Fig. 4 Photomicrographs showing fluid inclusions in quartz, cinnabar and barite. (a) Multiphase fluid inclusion in quartz, (L +V + anisotropic solid), (b) Two-phase fluid inclusion in quartz (L+V), with progressive growth of negative crystal forms, (c) Primary fluid inclusions in quartz growth zones, (d) Solid inclusion in quartz, identified as dolomite by Raman spectrometry, (e) Cinnabar inclusions in quartz (arrows), (f) Two-phase inclusions (L+V) in cinnabar, and (g) Cinnabar inclusions in barite (arrows).

Table 3 $\delta^{34}S$ (‰) values of cinnabar and barite from the Grübler orebody.

Sample	$\delta^{34}S$ (‰)	T [°C] *
ID-1-cinnabar	1.5	122.4±5.9
ID-1-barite	45.6	
ID-2-cinnabar	0.3	78.5±4.8
ID-2-barite	54.5	
ID-3-cinnabar	–0.5	69.4±4.6
ID-3-barite	56.3	
ID-4a-cinnabar	–0.7	
ID-4b-cinnabar	–0.3	

*Temperatures calculated by constants after Ohmoto and Rye (1979).

(Table 1), using the equation of Bodnar (1993). Total homogenisation (T_h) into the liquid phase between 160 and 218 °C was achieved only in quartz crystals (Fig. 5e), because of massive decrepitation in barite and cinnabar specimens. In a salinity vs. T_h diagram (Fig. 6) the quartz data show no specific trend and indicate precipitation from a rather heterogeneous fluid (Palinkaš et al., 2001). Isochores were calculated using the computer program ISOC (Fig. 7; Bakker, 2003) from the equation of state by Zhang and Frantz (1987) and a correction for the volumetric properties of quartz.

4.3. Laser Raman spectrometry (LRS)

Laser Raman spectroscopic measurements performed on the liquid phase of aqueous inclusions at room temperature revealed only the presence of water. Crystallites and solid carbonate inclusions were identified as dolomite on the basis of optical properties and Raman spectrometry (Fig. 4d). The Raman spectra also confirmed that the hydrate melting between –25.7 and –20.5 °C is hydrohalite (Dubessy et al., 1982), but the low-temperature salt hydrate could not be identified.

4.4. Bulk crush-leach analysis

Bulk crush-leach analysis and calculated ion concentrations reveal the predominance of Mg–Ca–Na–K±Li chlorides (Table 1). High concentrations of Mg and Ca reflect widespread metasomatism in the carbonate host rocks and saturation with respect to dolomite. The large charge imbalance (Q^+/Q^->1, Table 1) can be expected due to the inability of the method to analyse all dissolved species, notably sulphides and carbonates, but solid dolomite inclusion may also have contaminated the crush-leach analysis (see Channer and Spooner, 1992). Large differences in Cl^-/SO_4^{2-} ratio between barite, quartz and cinnabar could be explained in the same way, or by fluctuation of SO_4^{2-} due to barite precipitation. Potential source-rock reaction temperatures from the Na/K (Can, 2002), Na/Li (Verma and Santoyo, 1997), and Na/K/Ca geothermometers (Fournier and Truesdell, 1973) are compared with homogenisation temperatures in Table 2.

4.5. Sulphur isotopes

The isotopic compositions of ore-related sulphides from Idrija determined previously are: pyrite $\delta^{34}S$ = 1.6‰, metacinnabar $\delta^{34}S$ = +2.2‰, cinnabar $\delta^{34}S$ = –5.5 to +8.6‰ (n = 11, average –1.1‰, Ozerova et al., 1973). Cinnabar from the Grübler orebody has $\delta^{34}S$ = –7.57 to +7.46‰ (n = 9, average –2‰, Drovenik et al., 1991). Lavrić and Spangenberg (2001) obtained a wider range of values in pyrite from $\delta^{34}S$ = –15.6 to +20.0‰ (n = 36), and in cinnabar from $\delta^{34}S$ = –19.8 to +22.0‰ (n = 128). These data show a bimodal distribution with one maximum close to $\delta^{34}S$ = –7 and another at $\delta^{34}S$ = 0‰, attributed to contributions from a magmatic H_2S source and a sulphate component from Permo-Triassic seawater or evaporites. Gypsum lenses in the Upper Permian carbonates containing some cinnabar and native mercury (Placer and Čar, 1977) have $\delta^{34}S$ of +6.2 to +9.6‰ (Ozerova et al., 1973). The $\delta^{34}S$ values of gypsum from Permian to Middle Triassic host rocks vary from +12.3 to +16.4‰ (Lavrić and Spangenberg, 2001). Gypsum in the Lower Triassic dolomite (24.0‰), in lenses of oolithic limestones within shales (17.7‰), and in shales (28.7‰) were measured by Ozerova et al., 1973). Our $\delta^{34}S$ data from cinnabar of the deep Grübler orebody (Table 3; Fig. 8) fall in a narrow range from –0.7 to +1.5‰ (average +0.1‰). The data were superimposed on the diagram, Fig. 8 (after Lavrić and Spangenberg, 2001) for comparison. The average S-isotope values of cinnabar from the major stratigraphic sub-stages mimic the curve of the secular variation of the marine sulphates (Holser et al., 1988), which might be attributed to a contribution of evaporitic sulphate from each stratigraphic member.

The scarcity of barite limited the number of analyses on that mineral. The S-isotope values in barite are extraordinarily high ($\delta^{34}S$ = +45.6 to +56.3‰, average +52.1‰). Temperatures around 100 °C calculated from the isotope fractionation equation $1000 \ln \alpha_{barite-cinnabar} = 5.96/T^2 \times 10^6 + 6.0$ (±0.5; Ohmoto and Rye, 1979) are significantly lower than the fluid inclusion homogenisation temperatures (Table 2) and probably indicate that the texturally late barite was not precipitated in isotopic equilibrium with the cinnabar.

5. Discussion

The formation of a giant mercury-only deposit in a province of Hg-enriched polymetallic Fe–Ba–Pb–Zn–Ag deposits requires some special processes operating at Idrija. This may include the presence of a vapour-dominated hydrothermal system which enabled selective transport of mercury (White et al., 1971; Peabody and Einaudi, 1992).

5.1. Evidence for hydraulic fracturing

Abraded minerals and rock-fragments in open-cavity breccias of the Grübler orebody are interpreted to reflect a fast-flowing hydrothermal ore fluid, rather than post-ore percolation of meteoric water due to uplift of the area during the Alpine orogeny as suggested by Drovenik et al. (1991). Fluid inclusions in minerals cementing these

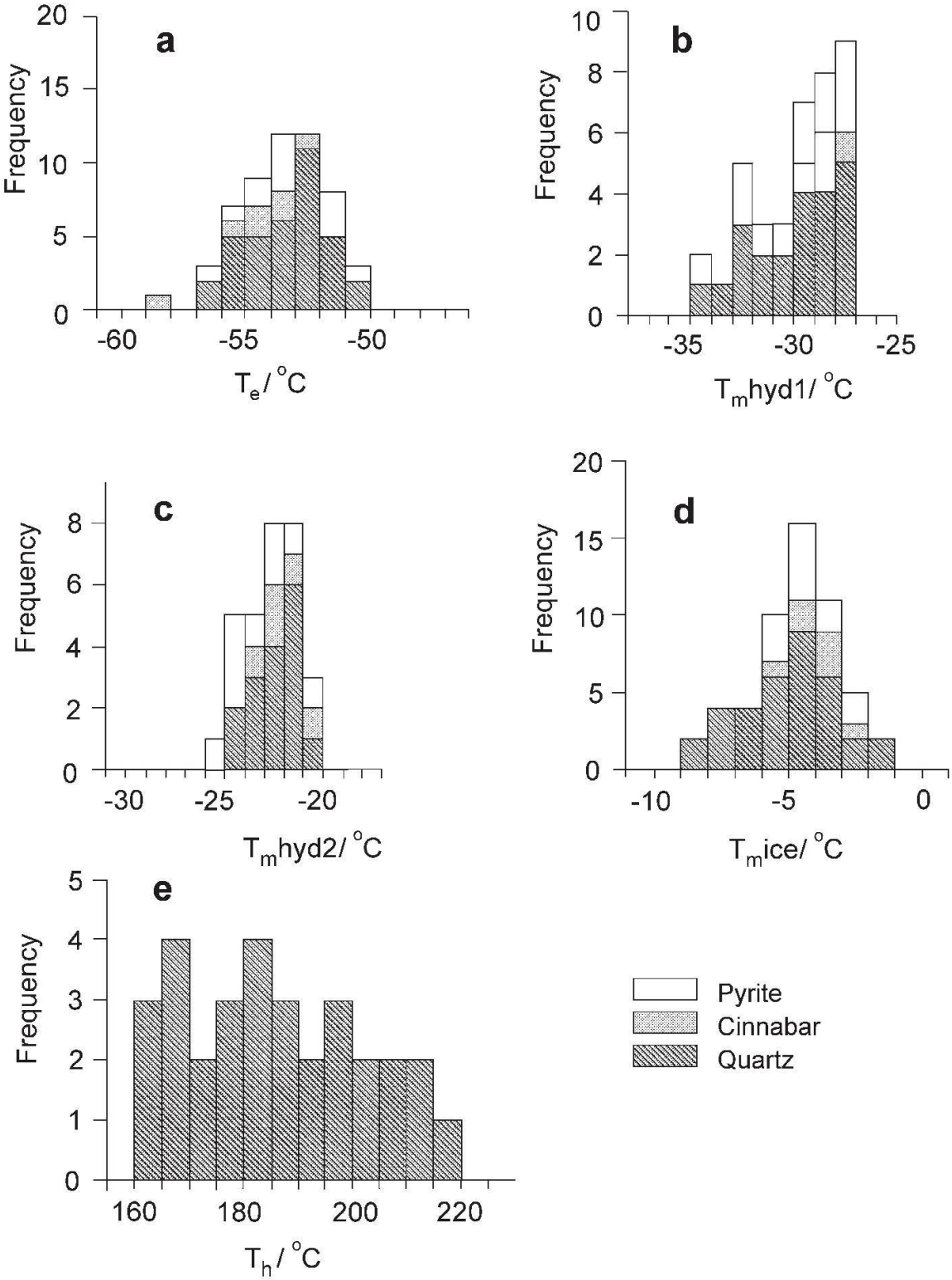

Fig. 5 Histograms showing frequency distributions of fluid inclusion data: (a) Eutectic temperatures, T_e, (b) Final melting temperatures of hydrate 1, $T_m$hyd1, (c) Final melting temperatures of hydrate 2, $T_m$hyd2, (d) Final melting temperatures of ice, $T_m$ice, and (e) Homogenisation temperatures, T_h.

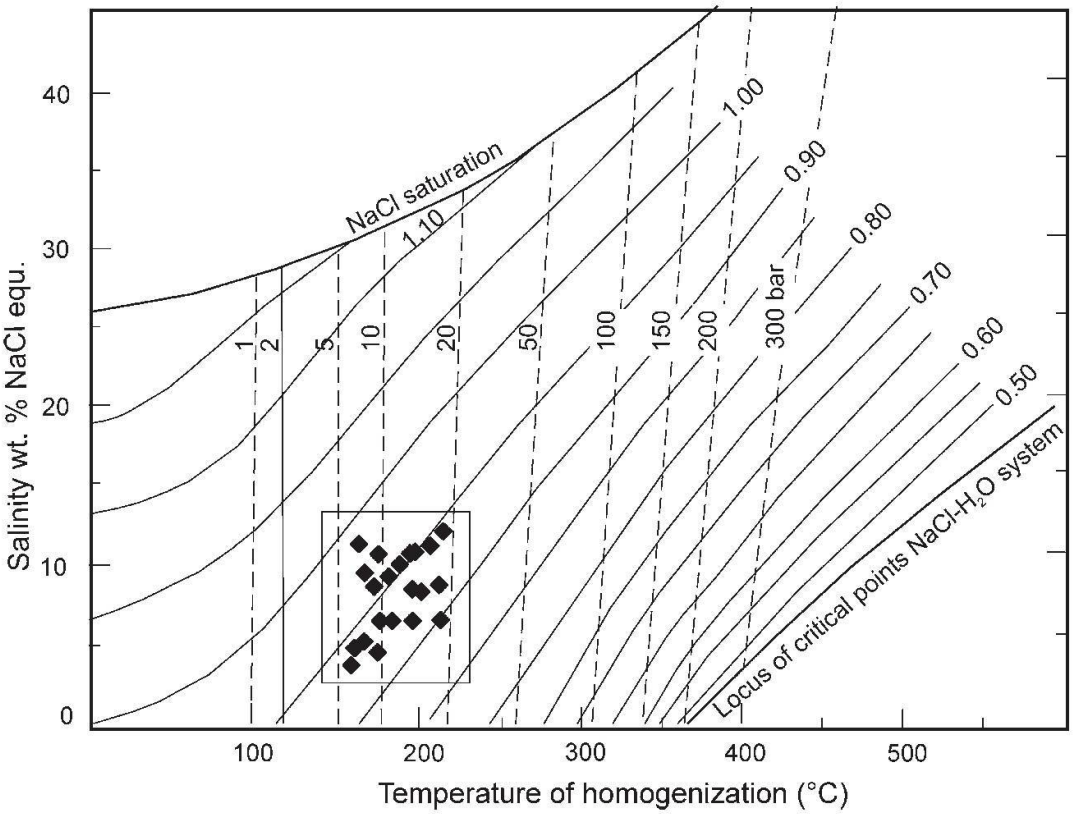

Fig. 6 Salinity vs. T_h diagram showing considerable scatter of fluid inclusion data indicating ore precipitation from a rather heterogeneous fluid. Isochores (fine solid lines, labelled in g·cm^{-1} for liquid density) and maximum H_2O vapour pressure at halite saturation (dashed lines) calculated with ISOC (Bakker, 2003).

rounded-clast breccias clearly prove their hydrothermal origin. Abrasion of the minerals therefore occured by fluidisation in a turbulent, rapidly ascending fluid.

The open-space fissures, cavities and breccias have developed perpendicular to the lowest main stress, σ_3 oriented parallel to the direction of the general rifting extension (Fig. 3, adopted after Placer, 1976). We therefore infer that these relatively narrow fissures were opened by hydraulic fracturing. Opening and brecciation occured when fluid pressure exceeded the sum of the least compressive stress plus the tensile strength of the rocks, leading to vertical expulsion of hot fluid into the colder overlying fractured carbonate rocks and permeable sandstones. This would have led to a drop in pressure and temperature by a combination of conductive cooling of the fluid in contact with the cold overlying rocks and adiabatic expansion of the initially over-pressured system towards hydrostatic fluid pressures.

5.2. Pressure and temperature of ore formation

The hydrocarbon-bearing fluid prior to ore deposition must have been under considerable pressure judging by the aqueous inclusion filling temperature between 160 °C and 218 °C. Even higher temperatures are indicated by the local presence of metacinnabar (stable above 315 °C; Potter and Barnes, 1978) and hydrothermally mobilised organic matter plotting in the HI vs. OI field of type-IV kerogen (indicating maturation temperatures up to ≈ 350 °C; Lavrić and Spangenberg, 2001; see also Kawka and Simoneit, 1994; Peters, 1986). The Na/K, Na/Li, Na/K/Ca thermometers (172 to 265 °C) also partly indicate temperatures greater that the inclusion filling temperatures, but they do not agree well and probably reflect partial fluid-rock equilibration at a deeper level. The partly contradictory estimates prevent a precise pressure correction and estimation of true temperatures of fluid trapping. Assuming the highest temperature of trapping to be 265 °C (obtained by the Na/K geothermometer), resulting pressures (Fig. 7) would greatly exceed the lithostatic pressure of ≈ 20 MPa corresponding to a thickness of ~ 750 m of sediments estimated to overlie the Grübler orebody at the time of ore formation (Placer, 1974–75). For the more reasonable temperatures range of 172–220 °C, the chloride-rich fluid might have attained adequate pressure required for hydraulic fracturing at $P_{fracturing} = (P_{lithostatic} + 2P_{hydrostatic})/3$ (Hubbert and Willis, 1957).

Hydrothermal maturation of organic matter by advection of heat by the fluid and possibly by oxidative maturation probably led to hydrocarbon gas generation (CH_4 and CO_2). The development of fluid overpressure is common in prograde basins with shale-rich sequences overlain by carbonates, for example in the Gulf of Mexico (Jones, 1970; Fowler, 1994). Gas formation at the base of the Idrija system may have temporarily increased the total fluid pressure even above the lithostatic threshold. High content of CH_4 (see maximum solubility isopleths of 1500, 2000 and 5000 ppm CH_4 in 15 wt% NaCl solution in Fig. 7, adapted from Hanor, 1980) will affect the slopes of isochores but this has not been evaluated for lack of data on the CH_4 concentrations in the inclusions. Nevertheless, the observation of high-temperature organic maturation implies that, upon pressure release during hydraulic fracturing, the hydrothermal system may have temporarily experienced vapour-dominated fluid flow, probably intermittent with aqueous solutions and liquid hydrocarbons.

5.3. Source, transport and deposition of petroleum, mercury, and sulphur

Speculations about the source of mercury in cinnabar deposits include mantle metasomatism (Fedorchuk, 1974; Ozerova, 1985), deep magmatic degassing of intrusions (Varekamp and Buseck, 1984; Rytuba and Heropoulos, 1992) or the sedimentary pre-enrichment in black shales possibly associated with coeval volcanic activity (Moiseyev, 1971; Saupé, 1990). Remobilisation from an Hg-rich sedimentary source seems to be the most probable option for the Idrija deposit. Huge masses of black shales are present at the base of the Langobardian fossil geothermal system. The mobilisation of hydrothermal petroleum and mercury must have been concurrent, initiated by infiltration of hot, chloride-rich brines into the black shales. The existence of three separate fluid phases — water, petroleum and vapour — seems realistic during hydraulic fracturing in the lower part of the geothermal system.

The formation of hydrothermal petroleum originated from immature refractory organic matter, producing polynuclear aromatic hydrocarbons (Simoneit, 1994). The abundance of such pyrolitic hydrocarbons with relative aliphatic depletion, without any isoprenoids detected in some samples, suggests that the Idrija host rocks were stained with hydrothermally matured petroleum (Lavrić and Spangenberg, 2001). The same characteristics were observed in the California Coast Range deposits (Wise et al., 1986; Peabody and Einaudi, 1992). The dominance of aromatics is attributed to reactions at more elevated temperatures than the standard oil window for petroleum generation in sedimentary basins (100–150 °C), or to preferential loss of other components with higher volatilities or solubilities (Douglas and Mair, 1965). Alternatively, sulphur may act as a catalyst in the formation of aromatics. The aque-

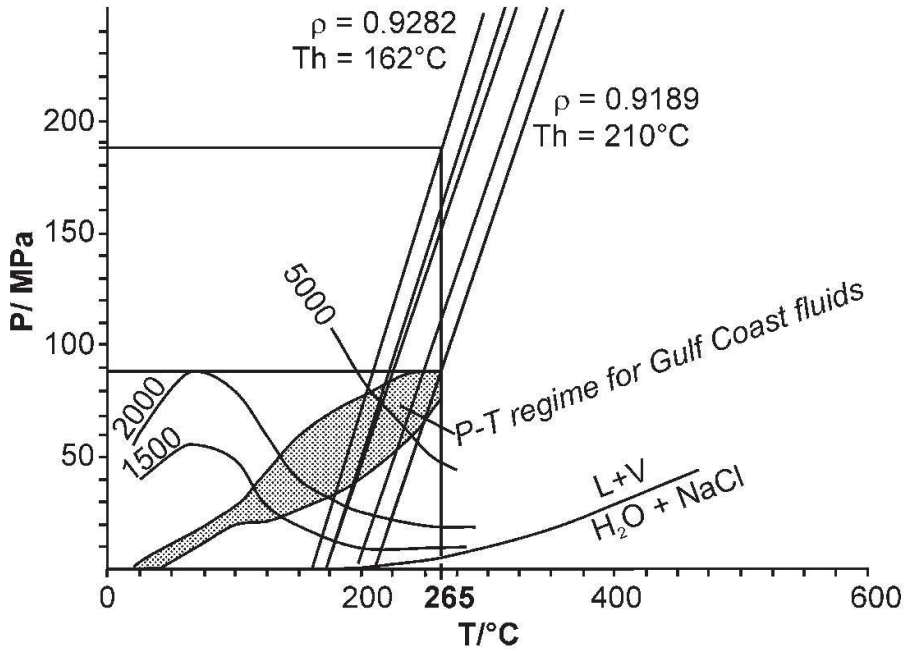

Fig. 7 P–T diagram showing isochores for binary aqueous fluids with 15 wt% NaCl, calculated using the computer program ISOC (Bakker, 2003), from the equation of state given by Zhang and Frantz (1987). Additional presence of 1500, 2000, 5000 ppm CH_4 in the saline fluid (isopleths for 15 wt% NaCl in H_2O) raises the bubble-point surface to higher minimum pressures (modified after Hanor, 1980). The influence of higher hydrocarbons and complex organics on T_h is unknown, but the slope of isochores will be less steep.

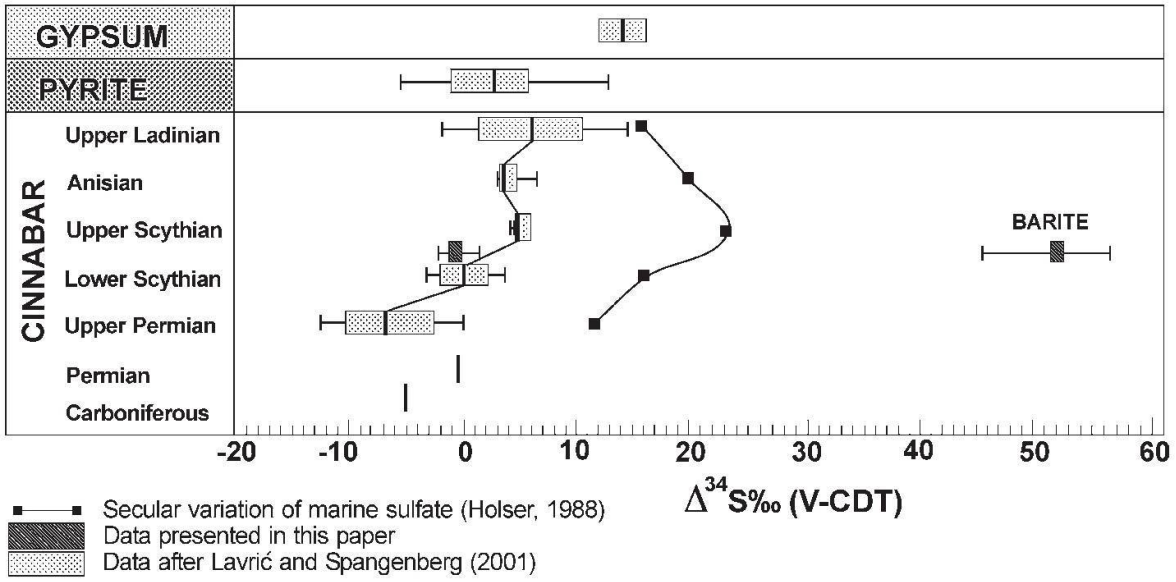

Fig. 8 Ranges and median values of $\delta^{34}S$ of cinnabar, pyrite and gypsum from the Idrija deposit (Lavrić and Spangenberg, 2001) with $\delta^{34}S$ of cinnabar and barite from the Grübler ore body shown for comparison. Barite is characterised by unusually heavy sulphur, which can be explained by disequilibrium Rayleigh fractionation during massive cinnabar precipitation or degassing during phase separation.

ous solubility of petroleum increases with temperature, approaching a critical regime with nearly complete miscibility (Price et al., 1983). Temperature and pressure decrease can lead to exsolution of liquid petroleum as well as hydrocarbon gas by phase separation from a C–O–H-rich aqueous fluid (Simoneit et al., 1992).

Mercury may have been transported by all three fluid phases, oil, gas or aqueous solution, before it was precipitated as cinnabar (dominant at depth) and native metal (a significant part of the resource in the upper levels of the hydrothermal system). Possible transporting species include Hg^0, bisulphide complexes such as $HgS(HS)^{2-}{}_{2aqu}$, and chloride complexes such as $HgCl_2{}^0$, besides possible organic complexes. Cinnabar precipitation from aqueous chloride brines can occur according to the following types of reactions:

$$HgCl_{2\,aqu} + HS^-_{aqu} = HgS_s + H^+ + 2Cl^- \quad (1)$$

precipitates cinnabar as a consequence of a pH rise, fluid dilution or a temperature drop of the aqueous phase, consistent with water-rich inclusions in crystalline cinnabar from the deep Grübler orebody. Assuming a bisulphide complex as Hg-carrier the reaction would be:

$$HgS(HS)^{2-}{}_2 = HgS_s + 2HS^- \quad (2)$$

which could lead to cinnabar deposition by partial sulphur loss due to boiling or oxidation, or also by dilution or a temperature decrease. Neutral Hg^0 could contribute to mercury transport in hot, reducing but S-poor aqueous fluids (Varekamp and Buseck, 1984) and may be the dominant form of mercury in CO_2–CH_4-rich gas or in liquid petroleum. Precipitation of cinnabar by

$$Hg^0 + H_2S = HgS_s + H_2 \quad (3)$$

will occur by addition of H_2S, or by removal of H_2 corresponding to an oxidation of the fluid system.

Considerable mercury concentrations occur in natural gas in the Pannonian Basin, which is characterised by high heat flow and likely magmatic underplating (Barić and Jungwirth, 1995). Natural gas from the Molve gas field (northern Croatia) contains 0.1–2.0 mg Hg/m^3, 7–1000 ppm H_2S, 10–24% CO_2 and a high content of mercaptane sulphur (Lukić et al., 2002; Ozerova et al., 1996). The reservoir temperature is 180–198 °C and the pressure prior to production was 50.5 MPa in the deepest hole at 3719 m. With estimated geological gas reserves of $39 \times 10^9\ m^3$, and assuming a concentration of 1 mg Hg/m^3, the total quantity of Hg in Molve is ~40,000 t Hg, which is about one third of the total production of the Idrija deposit.

Oxidation stabilises native mercury relative to cinnabar according to the reaction

$$Hg^0_l + H_2S = HgS_s + H_2 \quad (4)$$

explaining the formation of some liquid mercury by supergene weathering. However, it may also indicate primary deposition of liquid mercury in the upper part of the palaeogeothermal system, by simple cooling or interaction of neutral Hg^0 in the hydrocarbon gas or liquid petroleum phase with air, oxygen-bearing meteoric water or seawater sulphate in the brackish marshy environment (Fig. 2).

The sulphur source for cinnabar is uncertain, but clearly does not represent wholesale reduction of sulphates from marine fluids or the gypsum in the host sequence. The $\delta^{34}S$ data from the high-temperature HgS phase, metacinnabar, and the cinnabar data from the epigenetic Grübler orebody, located next to a likely major feeder fault of the Idrija system, are both very close to 0‰. These observations suggest that the Hg-introducing fluid carried a significant magmatic H_2S component. In addition, the sulphur in cinnabar probably includes a component derived from reduction of local evaporite sulphate, as indicated by the co-variation of cinnabar $\delta^{34}S$ with the marine evolution trend sulphur (Fig. 8; Ozerova et al., 1973; Lavrić and Spangenberg, 2001; cf. Holser et al., 1988). A progressive increase in $\delta^{34}S$ in cinnabar from the Upper Permian to the Upper Ladinian host rocks by 20‰, as observed by Lavrić and Spangenberg (2001), is consistent with increasing incorporation of an isotopically heavy sulphide component derived from hydrothermal reduction of sediment-derived sulphate, as the fluids ascended through the geothermal reservoir to the sediment-water interface. The extremely heavy sulphur isotope composition of hydrothermal barite is inconsistent with derivation from the moderately ^{34}S-enriched seawater or evaporite composition of the Permian to Triassic host sequence, and probably reflects closed-system isotope fractionation at low temperatures during the waning stages of mineralisation.

6. Summary and conclusions

The combination of published geological, fluid inclusion and sulphur isotope data from the entire Idrija deposit with new data from the fracture and breccia-hosted Grübler orebody has led to an improved model for the genesis of this giant mercury deposit. Idrija was formed in an aborted Ladinian rift related to the initial stage of Tethys opening. A trough was developed along subvertical normal faults, filled with Scythian, Anisian and Langobardian volcano-sedimentary formations overlying thick Permo-Carboniferous black shales, which represent a possible source of mercury and petroleum. The ore-forming palaeogeothermal system developed in response to widespread Middle Triassic subaerial, submarine and shallow intrusive bimodal magmatism. The geometry of the geothermal system was controlled by graben faults, so that the most productive orebodies with native mercury and stratiform cinnabar occur on the flanks of the trough, capped with a thin veneer of Langobardian volcano-sedimentary rocks. Precipitation of cinnabar started near the base of the geothermal system from a hot fluid, which may have been a near-critical mixed water-hydrocarbon phase that had scavenged mercury and hydrothermal petroleum at a deeper level. High fluid pressure caused hydraulic fracturing in the Scythian dolomites and the formation of the Grübler orebody containing fluidisation breccias and abraded minerals. The resulting drop in temperature and pressure gave rise to fluid immiscibility and separation of up to three phases: a chloride-rich aqueous liquid, liquid petroleum oil, and C–O–H-rich vapour that may have dominated in the higher portions of the geothermal system. Cinnabar was precipitated from the chloride-rich aqueous fluid and the liquid hydrothermal petroleum in the deeper Grübler orebody, using a combination of wall-rock derived sulphate and a possible magmatic sulphide component. Deposition of high-grade synsedimentary to syndiagenetic mercury ore occurred at the highest level of the geothermal system, in the black shales of a marshy environment close to the current sedimentation surface, incorporating a greater proportion of sulphur derived by sulphate reduction into cinnabar. Input of atmospheric oxygen into these upper levels have contributed to primary precipitation of elemental mercury, possibly suppressing cinnabar precipitation from Hg^0 contributed by an vapour phase ascending into the near-surface environment.

Acknowledgements

Special thanks go to R.J. Bakker for laser Raman spectroscopic measurements in the Institute of Geosciences, University of Leoben. We acknowledge financial support by the Swiss National Science Foundation through a SCOPES Grant 7KRPJ065483 in the framework of the GEODE collaboration funded by ESF. The Ministry of Science and Technology, Republic of Croatia, is acknowledged for sustenance of the research over the project 0119343. We are also grateful to J. Pamić for valuable suggestions on Dinaride geology, and V. Tari and S. Borojević-Šoštarić for their graphic contributions. Our sincere gratefulness is addresed to J. Schneider and M. Jébrak whose thorough reviews and suggestions made the manuscript more readable, and lastly to C. Heinrich for final reshaping of the text.

References

Bakker, R.J. (2003): Package FLUIDS 1. Computer programs for analysis of fluid inclusion data and for modeling bulk fluid properties. *Chem. Geol.* **194**, 3–23.

Barić, G. and Jungwirth, M. (1995): Origin of H_2S and organo-sulphur compounds in the gas-condensate field Stari Gradec (in Croatian). Proc. 1th Croatian Geological Congress, Opatija, Croatia 1, 47–50.

Berce, B. (1958): Geology of Idria mercury deposit. *Geologija*, Ljubljana, **4**, 5–62.

Brinck, J.W. and van Wambeke, L. (1975): World resources of mercury. 1st Congr. Inter. Del mercurio, Barcelona, 1974 (3/4), p. 39.

Blumer, M. (1975): Curtisite, idrialite, pendletonite, polycyclic aromatic hydrocarbon minerals: their composition and origin. *Chem. Geol.* **16**, 245–256.

Bodnar, R.J. (1993): Revised equation and table for determining the freezing point depression of H_2O–NaCl solutions. *Geochim. Cosmochim. Acta* **7**, 683–684.

Bottrell, S.H., Yardley, B.W.D. and Buckley, F. (1988): A modified crush-leach method for analysis of fluid inclusion electrolytes. *Bull. Mineral.* **111**, 279–290.

Čadež, F., Hudnik, V. and Gogala, A. (1981): Trace elements in the Idrija ore deposits country rocks (in Slovene with English summary). *Min. Metall. Q.*, Ljubljana, **28**, 33–43.

Čar, J. (1990): Angular tectonic-erosional unconformity in the deposit's part of the Idrija Middle Triassic tectonic structure (in Slovene with English summary). *Geologija*, Ljubljana, **31–32**, 267–284.

Can, I. (2002): A new improved Na/K geothermometer by artificial neural networks. *Geothermics* **31 (6)**, 751–760.

Channer, D.M. and Spooner, E.T.C. (1992): Analysis of fluid inclusion leachates from quartz by ion chromatography. *Geochem. Cosmochim. Acta* **56**, 249–259.

Colbertaldo, D. and Slavik, S. (1961): Il giacimento cinbrifero di Idria in Jugoslavia. *Rend. Soc. Mineral. Italiana*, Pavia, **17**, 1–22.

Dercourt, J., Zonenshain, L.P., Ricou, E.L., Kazmin, V.G., Le Pichon, X., Knipper, A.L., Grandjacquet, G., Sbortchikov, I.M., Geyssant, J., Lepvrier, C., Pechersky, D.H., Boulin, J., Sibuet, J.C., Savostin, L.A., Sorokhtin, O., Westphal, M., Bazhenov, M.L., Lauer, J.P. and Biju-Duval, B. (1986): Geological evolution of the Tethys belt from the Atlantic to the Pamir since the Lias. *Tectonophysics* **123**, 241–315.

Dewey, J.F., Pitman, W.C., Ryan, W.B.F. and Bonin, J. (1973): Plate tectonics and the evolution of the Alpine system. *Geol. Soc. Am. Bull.* **84**, 3137–3170.

Douglas, A.G. and Mair, B.J. (1965): Sulphur: Role in genesis of petroleum. *Science* **147**, 499–501.

Drovenik, M., Pleničar, M. and Drovenik, F. (1980): The origin of Slovene ore deposits (in Slovenian). *Geologija*, Ljubljana, **23**, 1–157.

Drovenik, M., Dolenec, T., Režun, B. and Pezdič, J. (1991): On the mercury ore from the Grübler orebody, Idrija. *Geologija*, Ljubljana, **33**, 397–446.

Dubessy, J., Audeoud, D., Wilkins, R. and Kosztolanyi, C. (1982): The use of the Raman microprobe MOLE in the determination of the electrolytes dissolved in the aqueous phase of fluid inclusions. *Chem. Geol.* **37**, 137–150.

Fedorchuk, V.P. (1974): Genetic and commercial types of mercury deposits. In: Congr. Int. Mercurio, Barcelona 1, 117–143.

Fowler, A.D. (1994): The role of geopressure zones in the formation of hydrothermal Pb–Zn Mississippi Valley type of mineralisation in sedimentary basins. In: Parnell, J. (ed.): Geofluids: Origin, Migration and Evolution of Fluids in Sedimentary Basins. *Geol. Soc. London Spec. Publ.* **78**, 293–300.

Fournier, R.O. and Truesdell, A.H. (1973): An empirical Na–K–Ca geothermometer for natural waters. *Geochim. Cosmochim. Acta* **37**, 1255–1276.

Giesemann, A., Jäger, H.J., Normann, A.L., Krouse, H.R. and Brand, W. (1994): On-line sulphur-isotope determination using an elemental analyzer coupled to a mass spectrometer. *Anal. Chem.* **66**, 2816–2819.

Hanor, J.S. (1980): Dissolved methane in sedimentary brines: potential effect on the PVT properties of fluid inclusions. *Econ. Geol.* **75**, 55–61.

Hernández, A., Jébrak, M., Higueras, P., Oyarzum, R., Morata, D. and Munha, J. (1999): The Almadén mercury mining district, Spain. *Mineral. Deposita* **34**, 539–548.

Higueras, P., Oyarzun, R., Lunar, R., Sierra, J. and Parras, J. (1999): The Las Cuevas deposit, Almadén district (Spain): unusual case of deep-seated advanced argillic alteration related to mercury mineralisation. *Mineral. Deposita* **34**, 211–214.

Holser, W.T., Schidlowski, M., Mckenzie, F.T. and Maynard, J.B. (1988): Geochemical cycles of carbon and sulphur. In: Gregor, C.B., Garrells, R.M., Mckenzie, F.T. and Maynard, J.B. (eds.): Chemical cycles in the evolution of the earth. Wiley, New York, 105–173.

Hubbert, M.K. and Willis, D.G. (1957): Mechanics of hydraulic fracturing. *Trans. Inst. Min. Metall. Pet. Eng.* **210**, 165–166.

Iglesias, G.J. and Pérez, L. (1989): Sobre las condiciones de removilización y precipitación de mercurio en el yacimiento de Almadén. III Congr. Geoquim. España I, 131–138.

Jones, P.H. (1970): Geothermal resources of the northern Gulph of Mexico basin. U.N. Symposium on the development and utilisation of geothermal resources, Pisa. Geothermics Spec. Issue 2, 14–26.

Jurković, I. and Pamić, J. (1999): Triassic rifting-related magmatism and metallogeny of the Dinarides. *Acta Geol.* **26 (1)**, 1–26.

Jurković, I. and Palinkaš, L. (2002): Discrimination criteria for assigning ore deposits located in the Dinaridic Palaeozoic-Triassic formations to Variscan or Alpidic metallogeny. In: Blundell, D.J., Neubauer, F. and von Quadt, A. (eds.): The timing and location of major ore deposits in an evolving orogen. *Geol. Soc. London Spec. Publ.* **204**, 229–245.

Kawka, O.E. and Simoneit, B.R.T. (1994): Hydrothermal pyrolysis of organic matter in the Guayamas basin: I. Comparison of hydrocarbon distribution in subsurface sediments and seabed petroleums. *Org. Geochem.* **22**, 947–978.

Kossmat, F. (1911): Geologie des Idrianer Quecksilberbergbaues. *J. geol. R.-A., Wien*, 339–384.

Lavrić, J.V. and Spangenberg, J. (2001): Geochemistry of the Idrija mercury deposit, Slovenia: insight from $\delta^{13}C$, $\delta^{18}O$, $\delta^{34}S$ and organic geochemical data. In: Piestrzyński et al. (eds.): Mineral Deposits at the Beginning of the 21st Century. A.A. Balkema, Rotterdam, 55–58.

Lavrić, J.V. and Spangenberg, J. (2003): Stable isotope (C, O, S) systematics of the mercury mineralization at Idrija, Slovenia: constraints on fluid source and alteration processes. *Mineral. Deposita* **38**, 886–899.

Lukić, M., Mađer, I. and Vađunec, J. (2002): Gas treatment plants: Molve I, II and III – A process power analysis. Petroleum Engineering School, Workshop 10: Gas Engineering, Inter-University Center. Dubrovnik, Croatia, 10–20.

Mioč, P. (2001): Characteristics of the Dinaric Carbonate Platform in Slovenia. 1st Sci. Meet. Carbonate platform or carbonate platforms of Dinarides, Abstracts, Zagreb, p. 57–58.

Mlakar, I. (1967): Relations between the lower and the upper structure of the Idrija ore deposit (in Slovenian). *Geologija Spec. Publ.*, Ljubljana, **10**, 87–126.

Mlakar, I. (1969): Krovna zgradba idrijsko-žirovskega ozemlja (Upper structure of the Idrija-Žirovski Vrh region). *Geologija*, Ljubljana, **12**, 5–72.

Mlakar, I. and Drovenik, M. (1971): Structural and genetic characteristics of the Idrija ore deposit (in Slovenian). *Geologija*, Ljubljana, **14**, 67–126.

Mlakar, I. (1974): An outline of production of the Idrija mercury mine through centuries, 1–40 (in Slovenian with English summary).

Mlakar, I. (1996): On the Marija Reka mercury deposit

and its comparison with the Litija and Idrija deposits from the aspect of plate tectonics (in Slovenian with English summary). *Geologija* **37–38**, 321–376.
Moiseyev, A.N. (1971): A non-magmatic source for mercury ore deposits? *Econ. Geol.* **66**, 591–601.
Neubauer, F., Genser, J. and Handler, R. (2000): The Eastern Alps: Result of a two-stage collision process. In: Neubauer, F. and Höck, V. (eds.): Aspects of Geology in Austria. *Mitt. Österr. Geol. Ges.* **92**, 117–134.
Ohmoto, H. and Rye, O.R. (1979): Isotopes of sulphur and carbon. In: Barnes, H.L. (ed.): Geochemistry of hydrothermal ore deposits, 2nd ed. John Wiley and Sons, 509–567.
Ozerova, N., Vinogradov, V.I., Mlakar, I., Fedorchuk, V.P. and Titov, I.N. (1973): Izotopni sostav seri v rudah nekatorih mestorozhdenii zapadnih chasti Sredizemnomorskogortutnogo pojasa (Isotope composition of sulphur in the ores of some ore deposits of the western Mediterranean mercury belt). In: Ocherki geohimii odelnih elementov. Nauka, Moscow, 275–310.
Ozerova, N. (1985): Sources of basic ore-forming elements in the mercury-antimony deposits. *Geologicky Zbornik-Geologica Carpathica* **36**, 4, 411–419.
Ozerova, N., Mashyanov, N.R., Pikovsky, YU.I., Ryzhov, V.V., Ganeev, A.A., Sholupov, S.E., Chernova, A.E., Leonthev, I.A., Zherebtsov, YU.D. and Dobryansky, L.A. (1996): Mercury in Gas and Oil deposits. 4th Int. Cong. on Mercury as a Global Pollutant. Hamburg, p. 336.
Palinkaš, A.L., Strmić, S., and Herlec, U. (2001): The ore-forming fluids in the Idrija mercury mine, Slovenia. In: Piestrzyński et al. (eds.): Mineral deposits at the beginning of the 21st Century. A.A. Balkema, Rotterdam, 321–324.
Pamić, J. (1984): Triassic magmatism of the Dinarides in Yugoslavia. *Tectonophysics* **109**, 273–307.
Pamić, J. (1993): Eoalpine to Neoalpine magmatic and metamorphic processes in the northwestern Vardar zone, the easternmost Periadriatic zone and the southwestern Pannonian Basin. *Tectonophysics* **226**, 503–518.
Pamić, J. and Jurković, I. (1997): Bosnia and Herzegovina In: Moores, E.M. and Fairbridge, R.W. (eds.): Encyclopedia of European and Asian Regional Geology. Chapman and Hall, London, 86–93.
Peabody, C.E. and Einaudi, M. (1992): Origin of Petroleum and Mercury in the Culver-Bear Cinnabar Deposit, Mayacmas District, California. *Econ. Geol.* **87**, 1078–1103.
Peters, K.E. (1986): Guidelines for evaluating petroleum source rock using programmed pyrolysis. *AAPG Bull.* **70**, 318–329.
Placer, L. (1974–75): The texture analysis of the epigenetic Grübler orebody in the Idrija ore deposit (in Slovenian). *Rudarsko-metalurški zbornik* **1**, 3–30.
Placer, L. (1976): Structural control of the epigenetic orebodies of the Idria ore deposit (in Slovenian). *Rudarsko-metalurški zbornik* **1**, 3–30.
Placer, L. and Čar, J. (1977): Middle Triassic structure of the Idrija region (in Slovenian). *Geologija*, Ljubljana, **20**, 141–166.
Potter II, R.W. and Barnes, H.L. (1978): Phase relations in the binary Hg–S. *Am. Mineral.* **63**, 1143–1152.
Price, L.C., Wenger, L.M., Ging, T. and Blount, C.W. (1983): Solubility of crude oil in methane as a function of pressure and temperature. *Org. Geochem.* **4**, 201–221.
Ramović, M., Kubat, I., Veljković, D., Kulenović, E. and Đurić, S. (1979): Obojeni i rijetki metali (Base and Rare metals). *Mineralne sirovine Bosne i Hercegovine*, Sarajevo, **3**, 7–121.
Rytuba, J.J., Rye, R.O., Hernández, A., Dean, J.A. and Arribas, A. Sr. (1989): Genesis of Almadén type mercury deposits, Almadén, Spain. Int. Geol. Cong., Washington, 2, p. 2741.
Rytuba, J.J. and Heropoulos, C. (1992): Mercury – an important byproduct in epithermal gold systems. Contributions to mineral commodities. *US Geol. Surv. Bull.* **1877**, D1-D8, Cited in: Hernández et al., (1999).
Schrauf, A. (1891): Über Metacinnabarit von Idria und dessen Paragenesis. *Jb. geol. R.-A., Wien*, 349–400.
Simoneit, B.R.T., Goodfellow, W.D. and Franklin, J.M. (1992): Hydrothermal petroleum at the seafloor and organic matter alteration in sediments of Middle Valley, Northern Juan de Fuca Ridge. *Appl. Geochem.* **7**, 257–264.
Simoneit, B.R.T. (1994): Organic matter alteration and fluids migration in hydrothermal systems. In: Parnell, J. (ed.): Geofluids: Origin, Migration and Evolution of Fluids in Sedimentary Basins. *Geol. Soc. London Spec. Publ.* **78**, 261–274.
Saupé, F. (1990): Geology of the Almadén mercury deposit, province of Ciudad Real, Spain. *Econ. Geol.* **85**, 482–510.
Saupé, F. and Arnold, M. (1992): Sulphur isotope geochemistry of the ores and country rocks at the Almadén mercury deposit, Ciudad Real, Spain. *Geochim. Cosmochim. Acta* **56**, 3765–3780 pp.
Spangenberg, J.E., Hunziker, J., Meisser, N. and Herlec, U. (1999): Compound specific analysis of the organic minerals hatchettite and idrialite in geodes, coal, and mineral deposits. In: Stanley, C.J. et al. (eds.): Mineral Deposits: Processes to Processing. A.A. Balkema, Rotterdam, 275–278.
Stur, D. (1872): Geologische Verhältnisse des Kessels von Idria in Krain. *Verh. geol., R.-A., Wien*, 235–240.
Tornquist, A. (1930): Perimagmatische Typen ostalpiner Erzlagerstätten. *Akad. d. Wiss., Mathem.-Naturw. Kl., Abt.I, 139 B, 3 und 4 Heft, Wien*, 291–308.
Varekamp, J.C. and Buseck, P.R. (1984): The speciation of mercury in hydrothermal systems, with applications to ore deposition. *Geochim. Cosmochim. Acta* **48**, 177–185.
Verma, P.S. and Santoyo, E. (1997): New improved equations for Na/K, Na/Li and SiO_2 geothermometers by outlier detection and rejection. *J. Volcanol. Geotherm. Res.* **79**, 9–23.
White, D.E., Muffler, L.P.J. and Truesdell, A.H. (1971): Vapor-dominated hydrothermal systems compared with hot-water systems. *Econ. Geol.* **66**, 75–97.
Wise, S.A., Campbell, R.M., West, W.R., Lee, M.L. and Bartle, K.D. (1986): Characterisation of polycyclic aromatic hydrocarbon minerals curtisite, idrialite and pentlandite using high-performance liquid chromatography, mass spectrometry and nuclear magnetic resonance spectroscopy. *Chem. Geol.* **54**, 339–357.
Zhang, Y.G. and Frantz, J.D. (1987): Determination of the homogenisation temperatures and densities of supercritical fluids in the system NaCl–KCl–$CaCl_2$–H_2O using synthetic fluid inclusions. *Chem. Geol.* **64**, 335–350.

Received 26 September 2003
Accepted in revised form 25 June 2004
Editorial handling: C. Heinrich